

Co monolayers and adatoms on Pd(100), Pd(111) and Pd(110): Anisotropy of magnetic properties

O. Šipr,^{1,*} S. Bornemann,² H. Ebert,² S. Mankovsky,² J. Vackář,¹ and J. Minář²

¹*Institute of Physics of the ASCR v. v. i., Cukrovarnická 10, CZ-162 53 Prague, Czech Republic*

²*Universität München, Department Chemie, Butenandtstr. 5-13, D-81377 München, Germany*

(Dated: September 16, 2018)

We investigate to what extent the magnetic properties of deposited nanostructures can be influenced by selecting as a support different surfaces of the same substrate material. Fully relativistic *ab initio* calculations were performed for Co monolayers and adatoms on Pd(100), Pd(111), and Pd(110) surfaces. Changing the crystallographic orientation of the surface has a moderate effect on the spin magnetic moment and on the number of holes in the *d* band, a larger effect on the orbital magnetic moment but sometimes a dramatic effect on the magnetocrystalline anisotropy energy (MAE) and on the magnetic dipole term T_α . The dependence of T_α on the magnetization direction α can lead to a strong apparent anisotropy of the spin magnetic moment as deduced from the X-ray magnetic circular dichroism (XMCD) sum rules. For systems in which the spin-orbit coupling is not very strong, the T_α term can be understood as arising from the differences between components of the spin magnetic moment associated with different magnetic quantum numbers m .

PACS numbers: 75.70.Ak, 75.30.Gw, 78.70.Dm, 73.22.Dj

Keywords: magnetism, anisotropy, nanosystems, XMCD

I. INTRODUCTION

The magnetic properties of surface deposited nanostructures have been in the ongoing focus of many experimental and theoretical investigations as they often exhibit interesting and sometimes unexpected phenomena. One of the main features in this context is that the local magnetic moments and their mutual interaction as well as the magnetocrystalline anisotropy energy (MAE) are in general different and often much larger in nanostructures than in corresponding bulk systems. Various aspects of the magnetism of many different nanostructures were studied in the past to identify the key factors which could then be used to tune the properties of such systems in a desired way. It has been known for some time that one such key factor is the coordination number, with smaller coordination numbers generally implying larger magnetic moments.^{1–3} However, coordination numbers alone do not fully determine magnetism of nanostructures. The chemical composition can play a significant role as well. An Fe monolayer, for instance, has a larger spin magnetic moment when deposited on Au(111) than when deposited on Pt(111), whereas for a Co monolayer it is *vice versa*.³ The situation is even more diverse for the MAE where different substrates may lead to different properties of systems of otherwise identical geometries. For example, Co₂ and Ni₂ dimers on Pt(111) have out-of-plane magnetic easy axis but the same dimers on Au(111) have an in-plane magnetic easy axis.³

Experimental research on magnetism of nanostructures relies heavily on the X-ray magnetic circular dichroism (XMCD) sum rules.^{4–6} The strength of these sum rules is that they give access to spin magnetic moments μ_{spin} and orbital magnetic moments μ_{orb} separately and in a chemically specific way.^{7,8} However, the XMCD spin sum rule does not provide μ_{spin} alone but only its combination

$\mu_{\text{spin}} + 7T_\alpha$, where T_α is the magnetic dipole term (for the magnetization \mathbf{M} parallel to the α axis, $\alpha=x, y, z$).⁷ For bulk systems, T_α can be usually neglected but for surfaces and clusters the T_α term can have significant influence, as it has been demonstrated experimentally^{9,10} and theoretically.^{11–13} The anisotropy of the magnetic dipole term was predicted on general grounds¹⁴ and some estimates concerning the magnitude of this anisotropy in non-cubic bulk systems were given based on atomic-like model Hamiltonians¹⁴ or on *ab initio* calculations.¹⁵

Magnetic nanostructures may be prepared by combining and arranging different magnetic elements on different substrates. In this respect one can also address surfaces of different crystallographic orientations. Thus, it is important to know how the magnetic properties can be controlled by selecting for the substrate crystallographically different surfaces of the same material and whether one can expect different effects for complete monolayers and for adatoms. Connected with this is the question about the effects on the T_α term, because XMCD is perhaps the most frequently used experimental technique in this field and it is desirable to know how T_α can influence the values of magnetic moments deduced from the XMCD sum rules. For planning and interpreting such experiments, it would be very useful not only to know the T_α values from *ab initio* calculations but also to have a simple intuitive interpretation of the T_α term.

In order to learn more about this, we undertook a systematic study of Co monolayers and adatoms on Pd(100), Pd(111), and Pd(110) surfaces. Fully relativistic *ab initio* calculations were performed to obtain μ_{spin} , μ_{orb} , and T_α for different magnetization directions. The MAE was determined for all these systems as well. The accuracy of an approximative expression for the T_α term was checked to see whether it captures the essential physics. It is shown in the following that monolayers and adatoms on

different crystallographic surfaces may have indeed quite different magnetic properties, especially as concerns the MAE. Moreover, it is also demonstrated how the dependence of the T_α term on the magnetization direction leads to a surprisingly strong apparent anisotropy of μ_{spin} as deduced from the XMCD sum rules.

II. METHODS

A. Investigated systems

We investigated Co monolayers on Pd(100), Pd(111) and Pd(110) and also Co adatoms on the same surfaces. The corresponding structure diagrams are shown in Fig. 1 (for adatoms, obviously only one Co atom is kept). Two hollow adatom positions are possible for the (111) surface, differing by the position of the adatom with respect to the sub-surface layer; we consider the fcc position in this work (unless specified otherwise).

The Pd substrate has fcc structure with lattice constant $a=3.89$ Å. To determine the distances between the Co atoms and the substrate, we relied in most cases on the “constant volume approximation”: the vertical Co–Pd interplanar distance $z_{\text{Co-Pd}}$ is taken as an average between the interlayer distance in bulk Pd and the interlayer distance in a hypothetical pseudomorphically grown fcc Co film compressed vertically in such a way that the atomic volume of Co is the same as in bulk Co.¹⁶ In addition we took also into account relevant experimental data and results of ab-initio geometry relaxations when available. For example, the constant volume approximation yields $z_{\text{Co-Pd}}=1.70$ Å for a Co monolayer on Pd(100) while we took $z_{\text{Co-Pd}}=1.65$ Å instead, following the surface X-ray diffraction experiment of Meyerheim *et al.*¹⁷ For the other two surfaces we used the constant volume approximation distances, namely, $z_{\text{Co-Pd}}=1.96$ Å for Co on Pd (111) and $z_{\text{Co-Pd}}=1.20$ Å for Co on Pd(110). In the case of the (111) surface we can compare our distance with an EXAFS-derived experimental distance $z_{\text{Co-Pd}}=2.02$ Å (Ref. 18) and with an *ab initio* equilibrium distance $z_{\text{Co-Pd}}=1.91$ Å (Ref. 19). It follows from this comparison that the constant-volume-approximation leads to reasonable distances.

Systems with interplanar distances as given above will be called systems with “optimized geometries”. Apart from that, we investigate for comparison also systems where the Co atoms are located in ideal positions of the underlying Pd lattice. For this we use the designation “bulk-like geometry”. The interplanar distances are summarized in Tab. I.

For adatoms we use the same $z_{\text{Co-Pd}}$ distances as for monolayers. This is a simplification because the constant volume approximation will work worse for adatoms than for monolayers. For example the *ab initio* $z_{\text{Co-Pd}}$ distance for a Co adatom on Pd(111) is 1.66 Å (Ref. 20) in contrast to our optimized geometry value of 1.96 Å. However, by using identical $z_{\text{Co-Pd}}$ distances for mono-

TABLE I. Vertical distances $z_{\text{Co-Pd}}$ between the plane containing Co atoms and plane containing Pd atoms for systems investigated in this study. The unit is Å.

surface	optimized geometry	bulk-like geometry
(100)	1.65	1.95
(111)	1.96	2.25
(110)	1.20	1.38

layers and adatoms, the net effect due to the change in Co coordination can be studied. It will be shown that the effect of varying the distances is in fact smaller than the effect of monolayer-to-adatom transition.

B. Computational scheme

The calculations were performed within the *ab initio* spin density functional framework, relying on the local spin density approximation (LSDA) with the Vosko, Wilk and Nusair parametrization for the exchange and correlation potential.²¹ The electronic structure is described, including all relativistic effects, by the Dirac equation, which is solved using the spin polarized relativistic multiple-scattering or Korringa-Kohn-Rostoker (SPR-KKR) Green’s function formalism²² as implemented in the SPR-TB-KKR code.²³ The potentials were treated within the atomic sphere approximation (ASA) and for the multipole expansion of the Green’s function, an angular momentum cutoff $\ell_{\text{max}}=3$ was used.

The electronic structure of Co monolayers on Pd surfaces was calculated by means of the tight-binding or screened KKR technique.²⁴ The substrate was modeled by slabs of 13–14 layers (i.e. a thickness of 17–27 Å, depending on the surface orientation), the vacuum was represented by 4–5 layers of empty sites. The adatoms were treated as embedded impurities: first the electronic structure of the host system (clean surface) was calculated and then a Dyson equation for an embedded impurity cluster was solved.²⁵ The impurity cluster contains 135 sites if not specified otherwise; this includes a Co atom, 50–60 Pd atoms and the rest are empty sites.

It should be stressed that the embedded clusters define the region where the electronic structure and potential of the host is allowed to relax due to the presence of the adatom and *not* the size of the considered system. In this respect the Green’s function approach differs from the often used supercell approach: there is an unperturbed host beyond the relaxation zone in the former approach while in the latter approach, the supercell is terminated either by vacuum or by another (interfering) relaxation zone pertaining to an adjacent adatom. The sizes of the embedded clusters and the sizes of the supercells thus have a different meaning and cannot be directly compared.

The magnetocrystalline anisotropy energy (MAE) is calculated by means of the torque $T_u^{(\hat{n})}$ which describes the variation of the energy if the magnetization direction

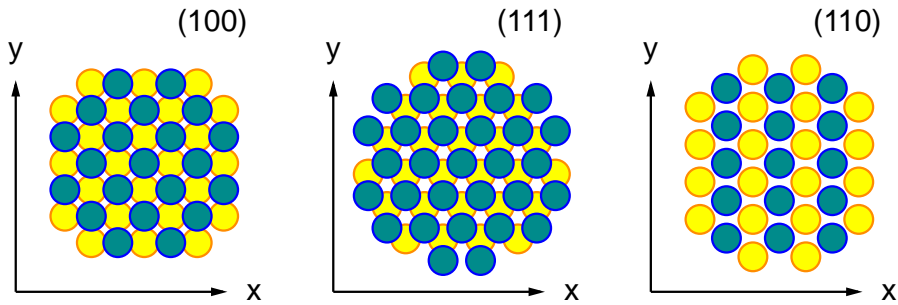


FIG. 1. (Color online) Structure diagrams for a Co monolayer on Pd(100), Pd(111) and Pd(110). The blue and yellow circles represent the Co and Pd atoms, respectively. The orientation of the x and y coordinates used throughout this paper is also shown.

\hat{n} is infinitesimally rotated around an axis \hat{u} . For uniaxial systems where the total energy can be approximated by

$$E(\theta) = E_0 + K_2 \sin^2(\theta) + K_4 \sin^4(\theta),$$

the difference $E(90^\circ) - E(0^\circ)$ is equal to the torque evaluated for $\theta = 45^\circ$.²⁶ The torque itself was calculated by relying on the magnetic force theorem.²⁷

Apart from the magnetocrystalline anisotropy induced by the spin-orbit coupling, the magnetic easy axis is also determined by the so-called shape anisotropy caused by magnetic dipole-dipole interactions. The shape anisotropy energy is usually evaluated classically by a lattice summation over the magnetostatic energy contributions of individual magnetic moments, even though it can be in principle obtained *ab initio* via a Breit Hamiltonian.²⁸ In this paper, we always deal only with the magnetocrystalline contribution to the magnetic anisotropy unless stated otherwise.

III. RESULTS

A. Magnetic moments and magnetocrystalline anisotropy

To assess the effect of selecting different crystallographic surfaces and of going from a monolayer to an adatom, we calculated magnetic moments, numbers of holes in the Co d band and the MAE for all these systems. The results are summarized in Tab. II. For each system, the data are shown first for the optimized geometry and then for the bulk-like geometry (numbers in the brackets). The x , y , and z superscripts in the column header labels indicate the direction of the magnetization \mathbf{M} .

The spin magnetic moment μ_{spin} and the number of holes in the d band n_h are shown only for $\mathbf{M} \parallel z$, because they are practically independent on the magnetization direction: by varying it, μ_{spin} can be changed by no more than 0.2 % and n_h by no more than 0.1 %. On the other hand, for μ_{orb} the differences can be quite large. The second in-plane magnetization direction $\mathbf{M} \parallel y$ was

investigated only for the (110) surface, because there is only very small “intraplanar anisotropy” for the (100) and (111) surfaces (this issue is addressed in more detail in Sec. III C). For bulk hcp Co we get $\mu_{\text{spin}} = 1.61 \mu_B$, $\mu_{\text{orb}} = 0.08 \mu_B$ and $n_h = 2.48$.

Changing the surface orientation has a moderate effect on μ_{spin} and n_h . The differences in μ_{spin} when going from one surface to another are at most 9 %. For n_h these differences are at most 5 %. However, the situation is quite different for μ_{orb} where the differences are 20–50 %. The sensitivity in μ_{orb} finds its counterpart in the sensitivity of the MAE. For example, the magnetic easy axis for a Co monolayer is in-plane for the (100) and (110) surfaces but out-of-plane for the (111) surface. For the adatom, the easy axis is in-plane for the (110) surface but out-of-plane for the (100) and (111) surfaces. So in this respect the choice of the crystallographic surface can have a dramatic influence.

Another finding emerging from Tab. II is that as concerns μ_{spin} , the difference between monolayers and adatoms is only quantitative in most cases. A surprisingly small difference in this respect is found for the (110) surface. As the same Co–Pd distances have been used for monolayers and adatoms, one observes here the net effect of the change in Co coordination. For μ_{orb} , the difference between monolayers and adatoms is obviously much larger than for μ_{spin} . For the MAE this difference can again be essential: The magnetic easy axis for a Co monolayer on Pd(100) is in-plane while for a Co adatom on the same surface it is out-of-plane. Similarly, the magnetic easy axis for a monolayer on Pd(110) is parallel to the y -axis while for an adatom it is parallel to the x -axis.

Changing the distance between Co atoms and the surface clearly affects the magnetic properties (cf. the values with and without brackets in Tab. II). However, it is noteworthy that the effect of geometry relaxation is smaller than the effect of the transition from the monolayer to the adatom.

We calculated also the magnetic shape anisotropy for the monolayers (classically, via a lattice summation, taking into account also moments on Pd atoms). As expected, this contribution favors always an in-plane

TABLE II. Magnetic properties of Co monolayers and adatoms on Pd(100), Pd(111), and Pd(110). The first column specifies whether the values are for a monolayer or for an adatom, the second column contains spin magnetic moment for the Co atom for $\mathbf{M}\parallel z$ (in units of μ_B), the third column contains number of holes in the d band for $\mathbf{M}\parallel z$. The fourth, fifth and sixth columns contain orbital magnetic moments for the Co atom for $\mathbf{M}\parallel z$, $\mathbf{M}\parallel x$, and $\mathbf{M}\parallel y$, respectively. The last three columns contain the MAE between indicated magnetization directions (in meV per Co atom). Numbers without brackets stand for systems with optimized Co–Pd distances, numbers in brackets stand for systems with a bulk-like geometry (see Sec. II A).

	$\mu_{\text{spin}}^{(z)}$	$n_h^{(z)}$	$\mu_{\text{orb}}^{(z)}$	$\mu_{\text{orb}}^{(x)}$	$\mu_{\text{orb}}^{(y)}$	$E^{(x)} - E^{(z)}$	$E^{(y)} - E^{(z)}$	$E^{(x)} - E^{(y)}$
Co on Pd(100)								
monolayer	2.09 (2.07)	2.45 (2.39)	0.132 (0.190)	0.203 (0.241)		-0.73 (-0.69)		
adatom	2.29 (2.32)	2.57 (2.53)	0.299 (0.610)	0.279 (0.473)		0.26 (2.69)		
Co on Pd(111)								
monolayer	2.02 (1.99)	2.43 (2.41)	0.135 (0.154)	0.136 (0.176)		0.36 (0.21)		
adatom	2.35 (2.34)	2.62 (2.52)	0.605 (0.780)	0.355 (0.575)		5.50 (6.38)		
Co on Pd(110)								
monolayer	2.15 (2.18)	2.50 (2.54)	0.192 (0.215)	0.183 (0.220)	0.210 (0.289)	-0.15 (-0.48)	-0.43 (-0.97)	0.28 (0.49)
adatom	2.20 (2.25)	2.49 (2.47)	0.270 (0.349)	0.347 (0.472)	0.201 (0.255)	-1.51 (-1.88)	1.10 (2.01)	-2.61 (-3.89)

orientation of the magnetization. For Co monolayers on Pd(100) and Pd(111), we get $E_{\text{dip-dip}}^{(x)} - E_{\text{dip-dip}}^{(z)} = -0.1$ meV. For Co monolayers on Pd(110), there is a small difference regarding the x and y directions: we get $E_{\text{dip-dip}}^{(x)} - E_{\text{dip-dip}}^{(z)} = -0.07$ meV and $E_{\text{dip-dip}}^{(y)} - E_{\text{dip-dip}}^{(z)} = -0.09$ meV. By comparing these values with the values shown in Tab. II, we see that the shape anisotropy energy is smaller in magnitude than the magnetocrystalline anisotropy energy and thus the shape anisotropy does not change the orientation of the magnetic easy axis as determined by the magnetocrystalline anisotropy.

B. Induced magnetic moments

Palladium is not magnetic as an element but it is quite polarizable.^{29,30} Spin magnetic moments induced in the Pd substrate by Co monolayers and adatoms are shown in Tab. III for all three surface orientations. In the case of Co monolayers, the induced moments are shown for the first three atomic layers of Pd below the Co layer [denoted as Pd(1), Pd(2) and Pd(3) in Tab. III]. Note that the interlayer distances are 1.95 Å, 2.25 Å and 1.38 Å for the (100), (111) and (110) surfaces, respectively. The relatively large μ_{spin} for the Pd(2) and Pd(3) sites in the case of the (110) surface reflects the relatively small interlayer distance for this crystallographic orientation.

In the case of adatoms, the description is formally more complicated because Pd atoms belonging to the same coordination shell around the Co atom are not all equivalent: some of them belong to the surface layer, some to the sub-surface layer and so on. In order not be over-

TABLE III. Spin magnetic moments for Pd atoms which are first, second and third nearest neighbors of Co atoms, in units of μ_B . As in Tab. II, the numbers without brackets stand for systems with optimized geometry and the numbers in brackets stand for systems with bulk-like geometry.

	Pd(1)	Pd(2)	Pd(3)
Co on Pd(100)			
monolayer	0.29 (0.25)	0.17 (0.16)	0.11 (0.10)
adatom	0.18 (0.15)	0.06 (0.06)	0.04 (0.04)
Co on Pd(111)			
monolayer	0.32 (0.25)	0.16 (0.15)	0.03 (0.06)
adatom	0.16 (0.12)	0.02 (0.02)	0.04 (0.03)
Co on Pd(110)			
monolayer	0.29 (0.29)	0.22 (0.24)	0.17 (0.19)
adatom	0.15 (0.15)	0.04 (0.05)	0.04 (0.04)

whelmed by too much data, we display here only moments averaged over all atoms of a given coordination shell. Symbols Pd(1), Pd(2), and Pd(3) in Tab. III stand now for the first, second, and third shell of Pd atoms around the Co adatom.

Moreover, we also calculated the orbital magnetic moments for the Pd atoms in all systems and we found that μ_{orb} amounts to about 8–17 % of the corresponding μ_{spin} .

In this section we deal only with magnetic moments on those Pd atoms which are close to the Co atoms. The issue of more distant Pd atoms and of the total charge contained in the polarization cloud is dealt with in the Appendix. Here, we would only like to stress that it follows from the analysis outlined in the Appendix that our model system is clearly adequate to yield reliable values of induced magnetic moments for the Pd(1), Pd(2), and Pd(3) sites.

C. Azimuthal dependence of MAE

In general, the MAE defined as the difference between total energies for in-plane and out-of-plane orientation of the magnetization will depend on the azimuthal angle ϕ . This dependence is often ignored but may sometimes be significant. In our case, the intraplanar MAE $E^{(x)} - E^{(y)}$ is quite comparable to $E^{(x)} - E^{(z)}$ or $E^{(y)} - E^{(z)}$ for the (110) surface (see Tab. II). To get a more complete picture, we inspect the azimuthal dependence of $E^{(\parallel)}(\phi) - E^{(z)}$, where $E^{(\parallel)}(\phi)$ is the total energy if \mathbf{M} is in the surface plane ($\theta=0^\circ$) with the azimuthal angle ϕ . Our results for a Co adatom on all three Pd surfaces are shown in Fig. 2. The data reported here were obtained for the bulk-like geometry but the trends would be similar for any $z_{\text{Co-Pd}}$ distance.

One can see from Fig. 2 that the $E^{(\parallel)}(\phi) - E^{(z)}$ curves follow the symmetry of the appropriate surface, as expected. The amplitude of these curves is the most interesting information here. For high-symmetry surfaces, it is almost negligible: 0.008 meV or 3 % of the average value for Co on Pd(100) and 0.06 meV or 1 % of the average value for Co on Pd(111). For the (110) surface, however, the amplitude is 2.6 meV and to speak about an average MAE does not make sense in this case, as illustrated by the fact that the magnetic easy axis is in-plane for $\phi = 0^\circ$ and out-of-plane for $\phi = 90^\circ$.

D. Relation between magnetic dipole term and m -decomposed spin magnetic moment

The spin magnetic moment sum rule for the $L_{2,3}$ edge XMCD spectra can be written for a sample magnetized along the α direction as⁷

$$\frac{3}{I} \int (\Delta\mu_{L_3} - 2\Delta\mu_{L_2}) dE = \frac{\mu_{\text{spin}} + 7T_\alpha}{n_h}, \quad (1)$$

where $\Delta\mu_{L_{2,3}}$ are the differences $\Delta\mu = \mu^{(+)} - \mu^{(-)}$ between absorption coefficients for the left and right circu-

larly polarized light propagating along the α direction, I is the integrated isotropic absorption spectrum, μ_{spin} is the local spin magnetic moment (only its d component enters here), n_h is the number of holes in the d band, and T_α is the magnetic dipole term related to the d electrons. T_α can be written as^{31,32}

$$\begin{aligned} T_\alpha &= -\frac{\mu_B}{\hbar} \langle \hat{T}_\alpha \rangle, \\ &= -\frac{\mu_B}{\hbar} \left\langle \sum_\beta Q_{\alpha\beta} S_\beta \right\rangle, \end{aligned} \quad (2)$$

where

$$Q_{\alpha\beta} = \delta_{\alpha\beta} - 3r_\alpha^0 r_\beta^0 \quad (3)$$

is the quadrupole moment operator and S_α is the spin operator. If z is the quantization axis, the eigenvalues of S_z are $\pm(1/2)\hbar$.

A more transparent expression for T_α can be obtained if the spin-orbit coupling can be neglected. Then one can write³²

$$\begin{aligned} \hat{T}_x &= \left(-\frac{\mu_B}{\hbar}\right) \hat{Q}_{xx} \hat{S}_z \quad \text{for } \mathbf{M} \parallel x, \\ \hat{T}_y &= \left(-\frac{\mu_B}{\hbar}\right) \hat{Q}_{yy} \hat{S}_z \quad \text{for } \mathbf{M} \parallel y, \\ \hat{T}_z &= \left(-\frac{\mu_B}{\hbar}\right) \hat{Q}_{zz} \hat{S}_z \quad \text{for } \mathbf{M} \parallel z, \end{aligned} \quad (4)$$

where \hat{Q}_{xx} , \hat{Q}_{yy} and \hat{Q}_{zz} are quadrupole moment components referred to the crystal (global) reference frame and \hat{S}_z is the spin component with respect to the local reference frame in which \bar{z} is identical to the spin quantization axis. We are interested in the expectation value of the \hat{T}_α operator acting on the d components of the wave function in the vicinity of the photoabsorbing site. Using for the sake of clarity a simplified two-component formulation instead of the full Dirac approach, the wave function can be expanded in the angular-momentum basis as

$$\psi_{E\mathbf{k}}(\mathbf{r}) = \sum_{\ell m} \sum_s a_{E\mathbf{k}\ell m}^{(s)}(r) Y_{\ell m}(\hat{\mathbf{r}}) \chi^{(s)} \quad (5)$$

to obtain

$$T_\alpha = \left(-\frac{\mu_B}{\hbar}\right) \int_{-\infty}^{E_F} dE \int_{\text{BZ}} d\mathbf{k} \langle \psi_{E\mathbf{k}} | \hat{Q}_{\alpha\alpha} \hat{S}_z | \psi_{E\mathbf{k}} \rangle. \quad (6)$$

Restricting ourselves just to the $\ell = 2$ component and omitting the corresponding subscript in $a_{E\mathbf{k}\ell m}^{(s)}(r)$, we get

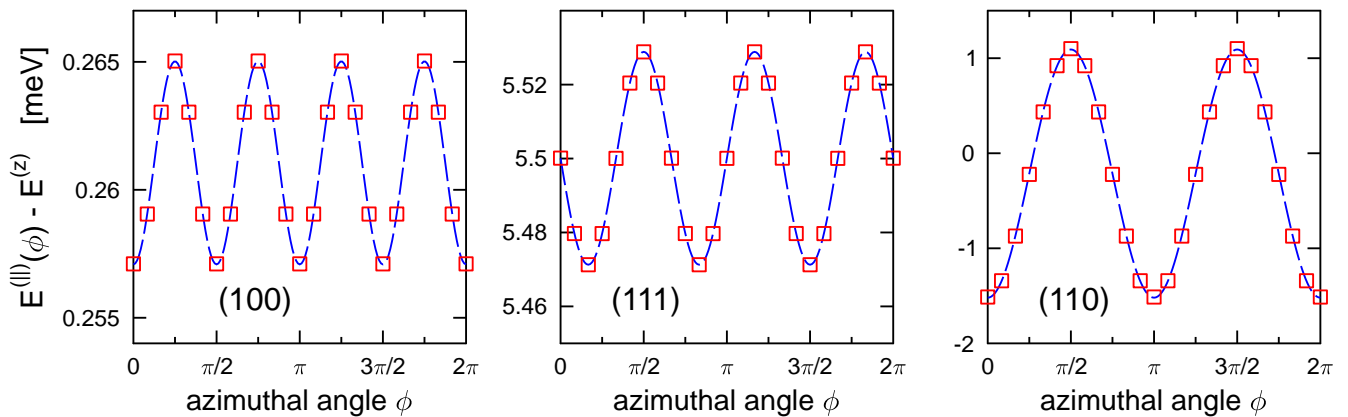


FIG. 2. (Color online) Difference between total energies for in-plane and out-of-plane magnetization for a Co adatom on Pd (100), (111), and (110) surfaces (bulk-like geometry). Points are results of the calculation, dashed lines are sinusoidal fits. The orientation of the x and y axes is as in Fig. 1.

$$\begin{aligned}
T_\alpha &= \left(-\frac{\mu_B}{\hbar}\right) \int_{-\infty}^{E_F} dE \int_{\text{BZ}} d\mathbf{k} \sum_{mm'} \sum_{ss'} \int d\mathbf{r} a_{E\mathbf{k}m}^{(s)*}(r) Y_{2m}^*(\hat{\mathbf{r}}) Q_{\alpha\alpha} a_{m'\mathbf{k}E}^{(s')}(r) Y_{2m'}(\hat{\mathbf{r}}) \langle \chi^{(s)} | \hat{S}_z | \chi^{(s')} \rangle \\
&= \left(-\frac{\mu_B}{\hbar}\right) \int_{-\infty}^{E_F} dE \int_{\text{BZ}} d\mathbf{k} \sum_{mm'} \int r^2 dr \left[a_{E\mathbf{k}m}^{\uparrow*}(r) a_{m'\mathbf{k}E}^{\uparrow}(r) - a_{E\mathbf{k}m}^{\downarrow*}(r) a_{m'\mathbf{k}E}^{\downarrow}(r) \right] \times \\
&\quad \langle Y_{2m} | \hat{Q}_{\alpha\alpha} | Y_{2m'} \rangle \frac{1}{2} \hbar \\
&= \frac{1}{2} (-\mu_B) \sum_{mm'} \left[N_{mm'}^{\uparrow} - N_{mm'}^{\downarrow} \right] \langle Y_{2m} | \hat{Q}_{\alpha\alpha} | Y_{2m'} \rangle, \tag{7}
\end{aligned}$$

where the spin-dependent number of states matrix $N_{mm'}^{(s)}$ is defined as

$$N_{mm'}^{(s)} = \int_{-\infty}^{E_F} dE \int_{\text{BZ}} d\mathbf{k} \int r^2 dr a_{E\mathbf{k}m}^{(s)*}(r) a_{m'\mathbf{k}E}^{(s)}(r).$$

The difference of the diagonal terms of $N_{mm}^{(s)}$ is just the spin magnetic moment decomposed according to the magnetic quantum number m ,

$$(-\mu_B) (N_{mm}^{\uparrow} - N_{mm}^{\downarrow}) = \mu_{\text{spin}}^{(m)},$$

with the sum of all the m components giving the total spin magnetic moment (of the d electrons, in our case). Therefore, if it was possible to restrict the sum (7) just to the terms diagonal in m , one would have

$$T_\alpha = \frac{1}{2} \sum_m \mu_{\text{spin}}^{(m)} \langle Y_{2m} | \hat{Q}_{\alpha\alpha} | Y_{2m} \rangle. \tag{8}$$

The procedure we employed above is essentially the one suggested by Stöhr,^{31,32} but we present it here in a more explicit way.

TABLE IV. Diagonal components of the quadrupole operator in the basis of real spherical harmonics. Non-diagonal components are all zero except for the components given in Eq. (9).

	Q_{xx}	Q_{yy}	Q_{zz}
$\langle Y_{xy} \hat{Q}_{\alpha\alpha} Y_{xy} \rangle$	$-\frac{2}{7}$	$-\frac{2}{7}$	$\frac{4}{7}$
$\langle Y_{yz} \hat{Q}_{\alpha\alpha} Y_{yz} \rangle$	$\frac{4}{7}$	$-\frac{2}{7}$	$-\frac{2}{7}$
$\langle Y_{3z^2-r^2} \hat{Q}_{\alpha\alpha} Y_{3z^2-r^2} \rangle$	$\frac{2}{7}$	$\frac{2}{7}$	$-\frac{4}{7}$
$\langle Y_{xz} \hat{Q}_{\alpha\alpha} Y_{xz} \rangle$	$-\frac{2}{7}$	$\frac{4}{7}$	$-\frac{2}{7}$
$\langle Y_{x^2-y^2} \hat{Q}_{\alpha\alpha} Y_{x^2-y^2} \rangle$	$-\frac{2}{7}$	$-\frac{2}{7}$	$\frac{4}{7}$

The coefficients $\langle Y_{2m} | \hat{Q}_{\alpha\alpha} | Y_{2m'} \rangle$ can be obtained by analytic integration. If we use the basis of *real* spherical harmonics, the only “cross-terms” which are non-zero are

$$\begin{aligned}
\langle Y_{x^2-y^2} | \hat{Q}_{xx} | Y_{3z^2-r^2} \rangle &= (2/7)\sqrt{3}, \\
\langle Y_{x^2-y^2} | \hat{Q}_{yy} | Y_{3z^2-r^2} \rangle &= -(2/7)\sqrt{3}. \tag{9}
\end{aligned}$$

Otherwise, only the diagonal terms $\langle Y_{2m} | \hat{Q}_{\alpha\alpha} | Y_{2m} \rangle$ are non-zero and we list them in Tab. IV (see also Refs. 14 and 31). Therefore, *in the absence of spin-orbit coupling*,

Eq. (8) presents an exact expression for T_z and an approximate expression for T_x and T_y [due to the existence of non-diagonal terms (9)]. As argued by Stöhr,³² the non-diagonal terms drop out of the sum in Eq. (7) for high symmetry systems.

Eq. (8) together with Tab. IV illustrate the common statement that the magnetic dipole term T_α is related to spin anisotropy: if the m -components of μ_{spin} are all identical, T_α is zero (in the absence of spin-orbit coupling). It is also evident from Eq. (8) and Tab. IV that the T_α term will generally depend on the magnetization direction α .

To get a more quantitative feeling of how the various contributions add together to generate T_α , we present in Tab. V the m -decomposed magnetic moment $\mu_{\text{spin}}^{(m)}$ and individual terms of the sum (8) for Co monolayers on Pd surfaces. One can see that the T_α term is formed by a competition between those m components which contain the α coordinate and those which do not (they contribute with an opposite sign, as it can be seen also from Tab. IV). In fact, this is what is meant by the statement that the T_α term describes the anisotropy of μ_{spin} .

Eq. (8) gives an intuitive insight into T_α provided that the underlying approximations — the neglect of the spin-orbit coupling and of the non-diagonal terms shown in Eq. (9) — are not too crude. To check this, we compare the values of T_α calculated via the exact relation in Eq. (2) and via the approximative Eq. (8). Special attention is paid to the differences between the T_α terms for different orientations of \mathbf{M} , because the $7(T_\alpha - T_\beta)$ quantities determine the apparent anisotropy of μ_{spin} as deduced from the XMCD sum rule in Eq. (1). The outcome for both monolayers and adatoms is summarized in Tab. VI. Let us recall that for bulk hcp Co, the magnetic dipole term is very small (we get $T_z = -0.002 \mu_B$). Note that all values presented in Tabs. V–VI were obtained from fully relativistic calculations, including the spin-orbit coupling.

One can see from our results that the approximative expression for T_α works quite well for the Co-Pd systems: quantitative deviations sometimes occur but the main trend is well maintained. One can expect that for systems with a strong spin-orbit coupling the deviations between Eqs. (2) and (8) will be larger.

The last two columns of Tab. VI contain the values of $7(T_x - T_z)$ and, for the case of the (110) surface, also of $7(T_y - T_z)$. These values are comparable to μ_{spin} which means that even though μ_{spin} practically does not depend on the magnetization direction at all, its combination $\mu_{\text{spin}} + 7T_\alpha$ probed by the XMCD sum rule may strongly depend on the magnetization direction.

IV. DISCUSSION

We investigated how the magnetic properties of Co adatoms and monolayers can be manipulated by selecting different supporting Pd surfaces. We found that this

has a moderate effect on μ_{spin} and n_h , larger effect on μ_{orb} and dramatic effect on the MAE and on the T_α term. For the adatoms the effect is larger than for the monolayers. Moreover, the transition from monolayers to adatoms has a larger effect than a moderate variation in the height of the Co layer above the substrate. If the spin-orbit coupling is not very strong, the T_α term can be understood as arising from a competition between those m -decomposed components of μ_{spin} which are associated with the α coordinate and those which are not.

In the past, the influence of the orientation of superlattices (multilayers) on magnetic properties was already investigated, however, the focus was mainly on the role of defects and interface abruptness.³³ Here, we deal with perfect monolayers and surfaces and investigate how sole selection of a different surface can affect various quantities related to magnetism. Likewise, the importance of the T_z term for an XMCD sum rules analysis has been highlighted before when it was found that the absolute value of $7T_z$ amounts to about 20 % of μ_{spin} for some low-dimensional systems¹² or that for atomic clusters μ_{spin} can show a different behavior with changing cluster size when compared to $\mu_{\text{spin}} + 7T_z$.¹³ In this study the importance of the *anisotropy* of the magnetic dipole term in nanostructures is stressed for the first time and it should be noted that the anisotropy of T_α which we highlight here is primarily connected with the breaking of the crystal symmetry at the surface and occurs even without spin-orbit coupling.

For the monolayers, the changes in μ_{spin} when going from one surface to another reflect the corresponding changes in the coordination numbers: μ_{spin} is largest for the (110) monolayer where each Co atom has got only two nearest neighboring Co atoms, next comes the (100) monolayer with four Co neighbors and the lowest μ_{spin} is obtained for the (111) monolayer with six Co neighbors. This complements an analogous trend found earlier for free¹ and supported clusters.^{2,3,34} The magnetic moments induced at individual Pd atoms are larger for Co monolayers than for Co adatoms, which reflects the fact that for monolayers, Pd atoms are polarized by more than one Co atom.

The large amount of data gathered here for quite a complete set of systems allows a comprehensive look at the relation between the MAE and the anisotropy of μ_{orb} . In this respect Bruno's formula³⁵

$$E^{(\alpha)} - E^{(\beta)} = -\frac{\xi}{4} \left[\mu_{\text{orb}}^{(\alpha)} - \mu_{\text{orb}}^{(\beta)} \right] \quad (10)$$

connecting the differences of total energies to the differences of orbital magnetic moments for two orientations of the magnetization, α and β , proved to be very useful³⁶ despite its limitations,³⁷ which become more severe in the case of multicomponent systems with large spin-orbit coupling parameter ξ for the non-magnetic component.^{38,39} To assess the situation for $3d$ - $4d$ alloys, we compare the differences $\Delta\mu_{\text{orb}}$ and ΔE , using all the appropriate values given in Tab. II. The outcome is

TABLE V. Spin magnetic moment decomposed according to the magnetic quantum number m together with the corresponding $T_\alpha^{(m)} = \frac{1}{2}\mu_{\text{spin}}^{(m)}\langle Y_{2m}|\hat{Q}_{\alpha\alpha}|Y_{2m}\rangle$ terms of the decomposition (8) for Co monolayers on Pd (optimized geometry). The sums of these components are shown in the last row for each system and they correspond to the total μ_{spin} , T_z , T_x , and T_y of the d electrons [evaluated using the approximative expression (8) in the case of T_α].

component	$\mu_{\text{spin}}^{(m)}$	$T_z^{(m)}$	$T_x^{(m)}$	$T_y^{(m)}$
Co on Pd(100)				
xy	0.319	0.092	-0.046	-0.046
yz	0.465	-0.066	0.133	-0.066
$3z^2 - r^2$	0.365	-0.104	0.052	0.052
xz	0.465	-0.066	-0.066	0.133
$x^2 - y^2$	0.449	0.128	-0.064	-0.064
sum	2.062	-0.018	0.009	0.009
Co on Pd(111)				
xy	0.339	0.097	-0.048	-0.048
yz	0.428	-0.061	0.122	-0.061
$3z^2 - r^2$	0.490	-0.140	0.070	0.070
xz	0.428	-0.061	-0.061	0.122
$x^2 - y^2$	0.339	0.097	-0.048	-0.048
sum	2.023	-0.069	0.034	0.034
Co on Pd(110)				
xy	0.397	0.113	-0.057	-0.057
yz	0.346	-0.049	0.099	-0.049
$3z^2 - r^2$	0.515	-0.147	0.074	0.074
xz	0.527	-0.075	-0.075	0.151
$x^2 - y^2$	0.343	0.098	-0.049	-0.049
sum	2.128	-0.060	-0.009	0.069

TABLE VI. Magnetic dipole term for Co monolayers and adatoms on Pd(100), Pd(111) and Pd(110) (optimized geometries) for different magnetization directions. For each system, the first line (“exact”) contains values calculated using Eq. (2) and the second line (“approx.,”) contains values calculated using Eq. (8). The T_y terms were evaluated only for the (110) surface.

		T_z	T_x	T_y	$7(T_x - T_z)$	$7(T_y - T_z)$
Co on Pd(100)						
monolayer	exact	-0.017	0.010		0.188	
	approx.	-0.018	0.009		0.184	
adatom	exact	-0.024	0.015		0.275	
	approx.	-0.026	0.013		0.276	
Co on Pd(111)						
monolayer	exact	-0.066	0.035		0.707	
	approx.	-0.069	0.034		0.723	
adatom	exact	-0.146	0.080		1.577	
	approx.	-0.154	0.077		1.618	
Co on Pd(110)						
monolayer	exact	-0.057	-0.008	0.068	0.339	0.872
	approx.	-0.060	-0.009	0.069	0.360	0.904
adatom	exact	-0.112	-0.020	0.141	0.644	1.768
	approx.	-0.117	0.011	0.106	0.900	1.566

shown in Fig. 3, together with a straight line representing Eq. (10). Here we take 85 meV for the spin-orbit coupling parameter ξ [which appears to be a rather universal value for Co as our calculations yield ξ of 85.4 meV, 84.5 meV, 84.9 meV and 85.1 meV for bulk hcp Co and for a Co monolayer on Pd(100), Pd(111) and Pd(110), respectively]. It follows from Fig. 3 that Bruno’s formula Eq. (10) works quite well for adatoms (albeit with

some “noise”) but not so well for monolayers, where relying solely on Eq. (10) might even lead to a wrong sign of the MAE. This may be connected with the fact that for monolayers, the MAE is generally not very large and hence small absolute deviations from the rule given in Eq. (10) can lead to large relative errors.

The sizable intraplanar anisotropy $E^{(x)} - E^{(y)}$ which we get for a Co monolayer on Pd(110) had to be expected

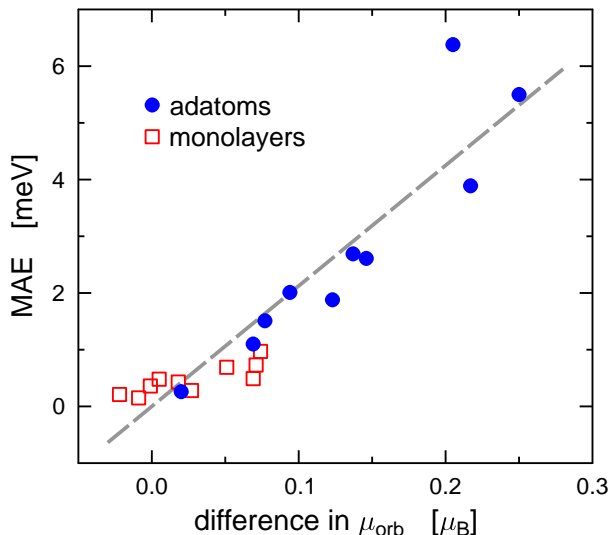


FIG. 3. (Color online) Dependence of the MAE for Co monolayers and adatoms on the difference of orbital magnetic moments for respective magnetization directions. The dashed line represents Bruno's formula in Eq. (10).

as this system could be viewed as a set of Co wires which are surely anisotropic in this respect. However, we get a very strong azimuthal dependence of the MAE also for the *adatom* on the (110) surface which is quite surprising as this can be only caused by the underlying substrate. The magnetic moments at Pd atoms are not very large (Tab. III), neither is the spin-orbit coupling parameter ξ for Pd in comparison to, say, *5d* elements. Thus, this seems to be yet another example of the extreme sensitivity of the MAE. At the same time, let us note that the calculated azimuthal dependence of the MAE can be accurately fitted by smooth sinusoidal curves (see Fig. 2) which indicates a very good numerical stability of the computational procedure.

The intraplanar anisotropy for a Co adatom on the Pd(111) surface can be compared to similar systems investigated in the past. In particular, for a Co adatom on Pt(111) the amplitude of the $E^{(\parallel)}(\phi) - E^{(z)}$ curve is about 2 % of the average value,⁴⁰ i.e., similar to the current case. For a 2×2 surface supercell coverage of Fe on Pt(111), this amplitude is 10–25 % (depending on the geometry relaxation)⁴¹ but this situation is already quite distinct from the isolated adatom case.

According to our calculations, a Co monolayer on Pd(100) has an in-plane magnetic easy axis, a Co monolayer on Pd(111) has an out-of-plane magnetic easy axis and the difference between the respective MAE values is about 1 meV, which can be seen as a measure of how much the out-of-plane magnetization is preferred by the Co/Pd(111) system in comparison with the Co/Pd(100) system. This is similar to what was calculated for Co/Pd multilayers: both Co_1Pd_3 (100) and Co_1Pd_2 (111) multilayers have an out-of-plane magnetic easy axis but the

MAE per unit cell is by about 0.9 meV larger for the (111) multilayer than for the (100) multilayer.⁴²

The theoretical values for the anisotropy of T_α shown in Tab. VI can be compared with experimental data for a similar system, namely, a single Co(111) layer sandwiched between two thick Au layers. By extrapolating results obtained via angle-dependent XMCD measurements, Weller *et al.*⁴³ obtained $7T_x = 0.43 \mu_B$ and $7T_z = -0.86 \mu_B$. Our values for a Co monolayer on Pd(111), $7T_x = 0.24 \mu_B$ and $7T_z = -0.46 \mu_B$ (see Tab. VI), are fully consistent with this.

We expect that our values for μ_{orb} will be systematically smaller than experimental values because we rely in the LSDA which usually underestimates μ_{orb} .^{44,45} The same may be also true for the MAE. However, this does not affect our conclusions.

We used potentials subject to the ASA which may limit the numerical accuracy of our results, particularly as concerns the MAE. On the other hand, our results do not differ too much from results of full-potential calculations, especially in the case of monolayers. For a Co monolayer on Pd(100), we get an in-plane magnetic easy axis with an MAE of -0.73 meV per Co atom while Wu *et al.*⁴⁶ obtained for the same $z_{\text{Co-Pd}}$ distance (1.65 Å) a theoretical MAE of -0.75 meV. Magneto-optic Kerr measurements¹⁷ as well as XMCD experiments⁴⁷ showed that the magnetic easy axis of ultrathin Co films on Pd(100) is indeed in-plane (the experiment includes also an in-plane contribution from the shape anisotropy). Note that the theoretical MAE of -0.18 meV given in Ref. 17 was obtained for a partially disordered Co monolayer simulating the growth conditions, so it cannot be directly compared to our results obtained for an ideal monolayer.

For a Co monolayer on Pd(111), we get a μ_{spin} value of $2.01 \mu_B$ in a Co ASA sphere with a radius of 1.46 Å while the full-potential calculations of Wu *et al.*⁴⁸ led to a μ_{spin} value of $1.88 \mu_B$ obtained within a Co muffin-tin sphere with a radius of 1.06 Å — both calculations thus again give consistent results. For Pd atoms just below the Co layer, we get a μ_{spin} value of $0.32 \mu_B$ in a sphere with a radius of 1.49 Å while the corresponding μ_{spin} value of Wu *et al.*⁴⁸ obtained within a sphere having a radius of 1.32 Å is $0.37 \mu_B$. In this last case, one has to bear in mind that Wu *et al.*⁴⁸ used a thin slab of only five Pd layers sandwiched between two Co layers which clearly favors a larger Pd polarization in comparison with just a single Co-Pd interface considered in this work.

For adatoms, the ASA may be more severe than for monolayers, nevertheless, the agreement between our calculations and the results obtained via a full potential calculation is pretty good (see the end of the Appendix). As a whole, the accuracy of our calculations is sufficient to warrant the conclusions which rely on comparing a large set of data and not only on results for a singular system.

It follows from our results that one can change the magnetic easy axis from in-plane to out-of-plane direction just by using as a substrate another surface of the same element. This could be used as yet another ingredient

for engineering the MAE of nanostructures, which has become a great challenge recently.⁴⁹ We also showed that the magnetic dipole T_α term can mimic a large anisotropy of μ_{spin} as determined from the XMCD sum rules. Hence, the anisotropy of T_α has to be taken fully into account when analyzing XMCD experiments on nanostructures.

V. CONCLUSIONS

Co monolayers and adatoms adsorbed on different surfaces of Pd exhibit quite different magnetic properties. The effect on μ_{spin} is moderate, the effect on μ_{orb} is larger while the effect on the MAE and on the magnetic dipole term T_α may be crucial. A surprisingly strong azimuthal dependence of the MAE is predicted for a Co adatom on Pd(110).

The dependence of T_α on the direction of the magnetization can lead to an apparent anisotropy of the spin magnetic moment as deduced from the XMCD sum rules. For systems with small spin-orbit coupling, the T_α term can be related to the differences between components of the spin magnetic moment associated with different magnetic quantum numbers.

ACKNOWLEDGMENTS

This work was supported by the Grant Agency of the Czech Republic within the project 108/11/0853, by the Bundesministerium für Bildung und Forschung (BMBF) Verbundprojekt Röntgenabsorptionsspektroskopie (05K10WMA) and by the Deutsche Forschungsgemeinschaft (DFG) via SFB 689. Stimulating discussions with P. Gambardella are gratefully acknowledged.

Appendix: Effect of the size of the relaxation zone

When studying the magnetism of adatoms, one should address the question to which extent the host around the adatom has to be allowed to polarize. Zeller showed²⁹ that the polarization cloud around a magnetic impurity in bulk Pd extends at least up to 1000 atoms. Šipr *et al.*⁵⁰ showed that the convergence of the MAE with respect to the slab thickness and/or with respect to the size of the supercell which simulates the adatom is much slower than the convergence of magnetic moments. In view of these facts, it is desirable to explore more deeply the situation for the systems considered in this work.

As a test case, we select a Co adatom on Pd(111). To facilitate the comparison with calculations done by other methods, we put the Co adatom in an hcp hollow site, with the vertical distance between the Co adatom and the Pd surface layer as $z_{\text{Co-Pd}}=1.64$ Å. Our system is thus similar to the system investigated by Błoński *et al.*²⁰ (the main difference with respect to Ref. 20 is that we do not consider any buckling of the substrate). To

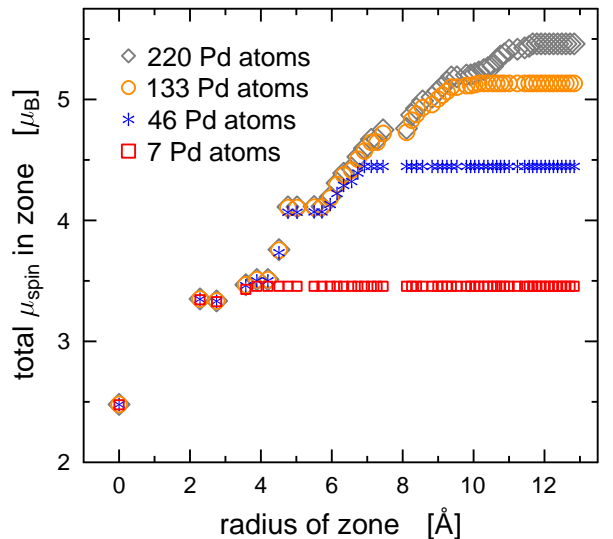


FIG. 4. (Color online) Sum of the spin magnetic moments at the Co adatom and at those substrate Pd atoms which are enclosed in hemispherical zones of the given radii, for four embedded cluster sizes (identified by numbers of Pd atoms contained in them).

check the convergence with respect to the size of the zone where the electronic structure is relaxed, we probed a series of embedded cluster sizes, starting with relaxing the electronic structure just in three Pd atoms (i.e., up to the distance of 2.3 Å from the Co adatom) and ending with relaxing it in 220 Pd atoms (up to 11.7 Å from the Co adatom). To safely accommodate this large embedded clusters, we model the Pd substrate by a slab of 19 layers [contrary to 13 layers used in other calculations involving the Pd(111) surface in this work]. The largest embedded cluster with 220 Pd atoms contains Pd atoms located within the fifth layer below the surface and comprises 329 sites altogether.

First we investigate the convergence of the spin magnetic moments. This can be achieved by inspecting the total μ_{spin} contained inside a hemisphere stretching from the adatom up to a certain radius. The dependence of this total μ_{spin} on the radius of the hemisphere forms an “integral magnetic profile”. This is presented in Fig. 4 for four embedded cluster sizes containing 7, 46, 133, and 220 Pd atoms, respectively. The total μ_{spin} for a sphere with zero radius is obviously just the μ_{spin} value of the Co adatom. With increasing sphere radius the spin magnetic moments of enclosed Pd atoms are added to it. If the radius of the hemisphere becomes larger than the radius of the embedded cluster, the total μ_{spin} obviously does not change any more because the Pd atoms outside the embedded impurity cluster are nonmagnetic.

It follows from Fig. 4 that the spin magnetic moment of the adatom as well as magnetic moments induced in the nearest Pd atoms are actually already well described by relatively small embedded clusters. However, the total

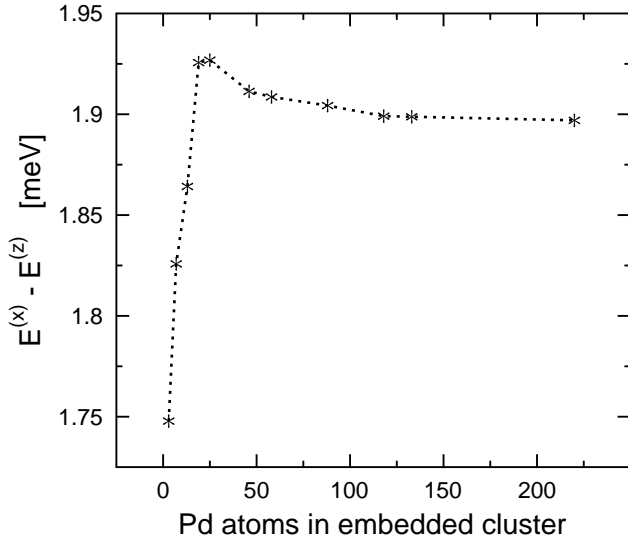


FIG. 5. The MAE of a Co adatom in an hcp position on Pd(111) for different sizes of the embedded clusters.

μ_{spin} converges only very slowly with increasing size of the relaxation zone because even quite distant Pd atoms still contribute with their non-zero μ_{spin} . Our results suggest that the magnetic moments on all the Pd atoms do not arise due to a direct interaction with the Co adatom. Rather, the adatom induces a magnetization in its nearest neighbors, then these further induce magnetization in the next coordination shell and so on. The emerging picture of how the magnetism spreads through the Pd host is thus consistent with the picture suggested by Polesya *et al.*³⁰ in terms of an exchange-enhanced magnetic susceptibility (see Fig. 4 of Ref. 30 and the associated text). A plot analogous to Fig. 4 could also be drawn for μ_{orb} exhibiting the same features as seen in Fig. 4.

Our results on the convergence of the magnetic moments may raise objections about the convergence of the MAE. If embedded clusters containing as much as 220

Pd atoms still do not fully account for the host polarization, can one get reliable results for the MAE, which is sensitive to the way the substrate is treated?⁵⁰ To check this, we calculated the MAE for a series of embedded cluster sizes (Fig. 5). One can see that in fact the MAE converges quickly with increasing size of the embedded cluster. Already with a relaxation zone including only 46 Pd atoms, which corresponds to a radius of the hemisphere of 6.9 Å containing Pd from up to the third Pd layer below the surface, the accuracy of the MAE is better than 1 %. This means that all the results presented in this work are well converged.

The data in Fig. 5 demonstrate that it is sufficient to include a rather small polarization cloud within the Pd host in order to get convergence in the MAE values. More distant Pd atoms do not contribute to the MAE, *even if they are magnetically polarized*. This conclusion is not in contradiction with an earlier result that reliable values of the MAE can be obtained only if the host is represented by slabs of at least ten layers⁵⁰ because that result concerned the total “physical” size of the model system while in this appendix we focus only on the size of the zone where the electronic structure is allowed to relax to the presence of an adatom (or of an adsorbed monolayer).

To complete this part, we should compare our results with the results of Błoński *et al.*²⁰ which were obtained by performing a plane-wave projector-augmented wave (PAW) calculation for a supercell comprising five-layers thick slabs and a 5×5 surface unit cell. As concerns the Co adatom itself, μ_{spin} and μ_{orb} for the in-plane magnetization direction and μ_{orb} for the out-of-plane magnetization direction are $2.48 \mu_B$, $0.15 \mu_B$, and $0.27 \mu_B$ in this work and $2.24 \mu_B$, $0.19 \mu_B$, and $0.22 \mu_B$ in Błoński *et al.*²⁰ As concerns the MAE calculated via the magnetic force theorem (torque method), it is 1.90 meV out-of-plane in this work and 0.72 meV out-of-plane in Błoński *et al.*²⁰ The value for the induced μ_{spin} in the nearest Pd atoms is $0.28 \mu_B$ in this work and $0.33 \mu_B$ in Błoński *et al.*²⁰ All these values are in good agreement, considering the differences between both approaches.

* sivr@fzu.cz; <http://www.fzu.cz/~sivr>

¹ O. Šipr, M. Košuth, and H. Ebert, Phys. Rev. B **70**, 174423 (2004).

² P. Mavropoulos, S. Lounis, R. Zeller, P. H. Dederichs, and S. Blügel, Appl. Physics A **82**, 103 (2006).

³ S. Bornemann, O. Šipr, S. Mankovsky, S. Polesya, J. B. Staunton, W. Wurth, H. Ebert, and J. Minár, Phys. Rev. B **86**, 104436 (2012).

⁴ P. Gambardella, A. Dallmeyer, K. Maiti, M. C. Malagoli, W. Eberhardt, K. Kern, and C. Carbone, Nature **416**, 301 (2002).

⁵ J. T. Lau, A. Föhlisch, R. Nietubyc, M. Reif, and W. Wurth, Phys. Rev. Lett. **89**, 057201 (2002).

⁶ P. Gambardella, S. Rusponi, M. Veronese, S. S. Dhesi, C. Grazioli, A. Dallmeyer, I. Cabria, R. Zeller, P. H. Dederichs, K. Kern, C. Carbone, and H. Brune, Science **300**, 1130 (2003).

⁷ P. Carra, B. T. Thole, M. Altarelli, and X. Wang, Phys. Rev. Lett. **70**, 694 (1993).

⁸ B. T. Thole, P. Carra, F. Sette, and G. van der Laan, Phys. Rev. Lett. **68**, 1943 (1992).

⁹ P. Gambardella, S. S. Dhesi, S. Gardonio, C. Grazioli, P. Ohresser, and C. Carbone, Phys. Rev. Lett. **88**, 047202 (2002).

¹⁰ S. Stepanow, A. Mugarza, G. Ceballos, P. Moras, J. C. Cezar, C. Carbone, and P. Gambardella, Phys. Rev. B **82**, 014405 (2010).

¹¹ R. Q. Wu and A. J. Freeman, Phys. Rev. Lett. **73**, 1994 (1994).

¹² M. Komelj, C. Ederer, J. W. Davenport, and M. Fähnle,

- Phys. Rev. B **66**, 140407(R) (2002).
- ¹³ O. Šipr, J. Minár, and H. Ebert, *Europhys. Lett.* **87**, 67007 (2009).
 - ¹⁴ J. Stöhr and H. König, *Phys. Rev. Lett.* **75**, 3748 (1995).
 - ¹⁵ M. Komelj, C. Ederer, and M. Fähnle, *Phys. Rev. B* **69**, 132409 (2004).
 - ¹⁶ P. Krüger, M. Taguchi, and S. Meza-Aguilar, *Phys. Rev. B* **61**, 15277 (2000).
 - ¹⁷ H. L. Meyerheim, M. Przybylski, A. Ernst, Y. Shi, J. Henk, E. Soyka, and J. Kirschner, *Phys. Rev. B* **76**, 035425 (2007).
 - ¹⁸ J. Miyawaki, D. Matsumura, A. Nojima, T. Yokoyama, and T. Ohta, *Surf. Sci.* **601**, 95 (2007).
 - ¹⁹ R. Wu, C. Li, and A. J. Freeman, *J. Magn. Magn. Materials* **99**, 71 (1991).
 - ²⁰ P. Błoński, A. Lehnert, S. Denner, S. Rusponi, M. Etzkorn, G. Moulas, P. Bencok, P. Gambardella, H. Brune, and J. Hafner, *Phys. Rev. B* **81**, 104426 (2010).
 - ²¹ S. H. Vosko, L. Wilk, and M. Nusair, *Can. J. Phys.* **58**, 1200 (1980).
 - ²² H. Ebert, D. Ködderitzsch, and Minár, *Rep. Prog. Phys.* **74**, 096501 (2011).
 - ²³ H. Ebert and R. Zeller, The SPR-TB-KKR package, <http://olymp.cup.uni-muenchen.de> (2006).
 - ²⁴ R. Zeller, P. H. Dederichs, B. Újfalussy, L. Szunyogh, and P. Weinberger, *Phys. Rev. B* **52**, 8807 (1995).
 - ²⁵ S. Bornemann, J. Minár, S. Polesya, S. Mankovsky, H. Ebert, and O. Šipr, *Phase Transitions* **78**, 701 (2005).
 - ²⁶ X. D. Wang, R. Q. Wu, D. S. Wang, and A. J. Freeman, *Phys. Rev. B* **54**, 61 (1996).
 - ²⁷ J. B. Staunton, L. Szunyogh, A. Buruzs, B. L. Gyorffy, S. Ostanin, and L. Udvardi, *Phys. Rev. B* **74**, 144411 (2006).
 - ²⁸ S. Bornemann, J. Minár, J. Braun, D. Koedderitzsch, and H. Ebert, *Solid State Commun.* **152**, 85 (2012).
 - ²⁹ R. Zeller, *Modelling Simul. Mater. Sci. Eng.* **1**, 553 (1993).
 - ³⁰ S. Polesya, S. Mankovsky, O. Šipr, W. Meindl, C. Strunk, and H. Ebert, *Phys. Rev. B* **82**, 214409 (2010).
 - ³¹ J. Stöhr, *J. Electron. Spectrosc. Relat. Phenom.* **75**, 253 (1995).
 - ³² J. Stöhr, *J. Magn. Magn. Materials* **200**, 470 (1999).
 - ³³ C. H. Lee, R. F. C. Farrow, C. J. Lin, E. E. Marinero, and C. J. Chien, *Phys. Rev. B* **42**, 11384 (1990).
 - ³⁴ O. Šipr, S. Bornemann, J. Minár, S. Polesya, V. Popescu, A. Šimůnek, and H. Ebert, *J. Phys.: Condens. Matter* **19**, 096203 (2007).
 - ³⁵ P. Bruno, *Phys. Rev. B* **39**, 865 (1989).
 - ³⁶ H. A. Dürr, G. Y. Guo, G. van der Laan, J. Lee, G. Lauhoff, and J. A. C. Bland, *Science* **277**, 213 (1997).
 - ³⁷ P. Ravindran, A. Kjekshus, H. Fjellvåg, P. James, L. Nordström, B. Johansson, and O. Eriksson, *Phys. Rev. B* **63**, 144409 (2001).
 - ³⁸ C. Andersson, B. Sanyal, O. Eriksson, L. Nordström, O. Karis, D. Arvanitis, T. Konishi, E. Holub-Krappe, and J. Hunter Dunn, *Phys. Rev. Lett.* **99**, 177207 (2007).
 - ³⁹ O. Šipr, J. Minár, S. Mankovsky, and H. Ebert, *Phys. Rev. B* **78**, 144403 (2008).
 - ⁴⁰ S. Bornemann, J. Minár, J. B. Staunton, J. Honolka, A. Enders, K. Kern, and H. Ebert, *Eur. Phys. J. D* **45**, 529 (2007).
 - ⁴¹ M. Tsujikawa, A. Hosokawa, and T. Oda, *J. Phys.: Condens. Matter* **19**, 365208 (2007).
 - ⁴² K. Kyuno, J. Ha, R. Yamamoto, and S. Asano, *J. Phys.: Condens. Matter* **8**, 3297 (1996).
 - ⁴³ D. Weller, J. Stöhr, R. Nakajima, A. Carl, M. G. Samant, C. Chappert, R. Mégy, P. Beauvillain, P. Veillet, and G. A. Held, *Phys. Rev. Lett.* **75**, 3752 (1995).
 - ⁴⁴ O. Hjortstam, J. Trygg, J. M. Wills, B. Johansson, and O. Eriksson, *Phys. Rev. B* **53**, 9204 (1996).
 - ⁴⁵ S. Chadov, J. Minár, M. I. Katsnelson, H. Ebert, D. Ködderitzsch, and A. I. Lichtenstein, *Europhys. Lett.* **82**, 37001 (2008).
 - ⁴⁶ R. Wu, L. Chen, and A. J. Freeman, *J. Magn. Magn. Materials* **170**, 103 (1997).
 - ⁴⁷ M. Sawada, T. Tagashira, K. Furumoto, T. Ueno, A. Kimura, H. Namatame, and M. Taniguchi, *J. Electron. Spectrosc. Relat. Phenom.* **184**, 280 (2011).
 - ⁴⁸ R. Wu, C. Li, and A. J. Freeman, *J. Magn. Magn. Materials* **99**, 71 (1991).
 - ⁴⁹ S. Ouazi, S. Vlačić, S. Rusponi, G. Moulas, P. Bulushek, K. Halleux, S. Bornemann, S. Mankovsky, J. Minár, J. B. Staunton, H. Ebert, and H. Brune, *Nature Communications* **3**, 1313 (2012).
 - ⁵⁰ O. Šipr, S. Bornemann, J. Minár, and H. Ebert, *Phys. Rev. B* **82**, 174414 (2010).